Composites Part B 303 (2025) 112599

Contents lists available at ScienceDirect

Composites Part B

journal homepage: www.elsevier.com/locate/compositesb

Microstructure and thermal properties of nano-SiO_2 reinforced 3D printed multiscale PEEK composites

Nayan Dhakal [a,b,*], Cayetano Espejo [b], Ardian Morina [b], Nazanin Emami [a,**]

[a] Polymer-tribology Group, Division of Machine Elements, Luleå University of Technology, SE, 97187, Luleå, Sweden
[b] Institute of Functional Surfaces, School of Mechanical Engineering, University of Leeds, LS2 9JT, Leeds, United Kingdom

ARTICLE INFO

Handling Editor: Dr Uday Vaidya

Keywords:
3D printing
Polymers
PEEK
SiO_2
Nanoparticles
Microstructure

ABSTRACT

Additive manufacturing (AM) is growing as a resource-efficient and economical processing technique for polymer-based materials. In recent years, substantial advancements have been made in the fused filament fabrication (FFF) of high-performance polyether-ether-ketone (PEEK). However, there is a notable lack of information in the existing literature on the 3D printing of nanoparticle-filled PEEK composites. In this study, PEEK-based composite filaments filled with nanoscale silicon dioxide (SiO_2) and microscale short carbon fibers (SCF) were successfully fabricated using melt compounding and 3D printing using FFF. The addition of 2 wt% nano-SiO_2 significantly enhanced interfacial bonding, reduced internal porosity, and improved the microstructure of SCF-PEEK composites. Tomography and microstructure analysis revealed a uniform distribution of fibers. Thermal and structural analysis confirmed that the chemical integrity of the PEEK matrix remained intact during the filament processing and 3D printing. Nano-SiO_2 enhanced the thermal decomposition temperatures and improved the crystallization behavior of SCF-PEEK. Multiscale composites exhibited up to 40 % and 11 % increments in stiffness compared to neat PEEK and SCF-PEEK, respectively. Overall, SiO_2 improved the microstructure, thermal properties, and dynamic modulus of printed SCF-PEEK composites. The findings in this study demonstrate that nano-SiO_2 is a promising filament filler for 3D printing of PEEK composites.

1. Introduction

Additive manufacturing (AM) or three-dimensional (3D) printing, primarily extrusion-based fused filament fabrication (FFF) of polymers has attracted considerable attention with a focus on optimized material usage and reduced production cycles of lightweight functional parts with enhanced sustainability. The processing difficulties of high-performance polymers in FFF due to their high processing temperatures and complex structure-property relationships are often challenging [1]. Recently, advancements in FFF technology have enabled the enhanced printability of high-performance polymers like polyether-ether-ketone (PEEK) [1,2]. PEEK is a semicrystalline polymer with excellent mechanical strength, high thermal stability, wear resistance, and corrosion resistance. PEEK and its composites are known to possess strategic importance in demanding applications with significant interests as load-carrying components [3,4].

In FFF printing of PEEK-based composites, short carbon fibers (SCF) are the most investigated fillers due to their high specific strength and excellent reinforcing properties [5–7]. Lv et al. [7,8] exhibited that the SCF content highly influences the tensile properties, microstructure, and crystallization behavior of 3D printed SCF-PEEK. The findings suggest that 5–10 wt% microscale SCF in PEEK can produce composites with superior mechanical and thermal properties compared to neat PEEK. Similarly, our previous work exhibited that 10 wt% SCF in PEEK is optimal for a significant improvement in tensile modulus and tribological performance. A 37 % reduction in coefficient of friction and minimized adhesive wear were achieved compared to printed neat PEEK [9]. Rodzeń et al. [5] printed SCF-PEEK mold inserts via FFF for the injection molding of commodity polymers, demonstrating the capability of 3D printing to produce PEEK composites for demanding engineering parts.

On the other hand, the performance quality of SCF-PEEK composites produced by FFF is often compromised due to the complexity of filament fabrication, void formation, flow instability, nozzle clogging, and uncontrolled fiber orientation [8,10–12]. The fiber-matrix interactions, interlayer bonding, and crystallization behavior can be influenced by the temperature gradients susceptible to the FFF technique [7,13]. The

* Corresponding author. Polymer-tribology Group, Division of Machine Elements, Luleå University of Technology, SE, 97187, Luleå, Sweden.
** Corresponding author.
E-mail addresses: nayan.dhakal@associated.ltu.se (N. Dhakal), nazanin.emami@ltu.se (N. Emami).

https://doi.org/10.1016/j.compositesb.2025.112599
Received 10 January 2025; Received in revised form 30 April 2025; Accepted 3 May 2025
Available online 5 May 2025

influence of chamber temperature on crystallization behavior and interlayer adhesion of SCF-PEEK was studied earlier [5]. The results showed that the temperature highly influenced the degree of crystallinity and formation of PEEK crystals. Void formation acts as a primary cause for the deterioration of mechanical properties of FFF-PEEK and its composites [2,14]. X-ray micro-computed tomography revealed that the introduction of fillers can increase the internal defects and pore volume fractions of printed composites [12,15]. It has been further realized that this often introduces anisotropy on the printed parts and increases the complexity of failure modes [16]. Therefore, it is crucial to understand the void formation, distribution of fillers, and its impact on the properties of printed composites.

Moreover, improved material design and processing methodology could further expand the range of applications for 3D printed PEEK composites. Adding nanoscale constituents that improve the microstructure of SCF-PEEK would help reach the goal of printing PEEK composites with superior performance. Consequently, increasing interest has been generated recently in developing PEEK-based nanocomposite filaments [17–20]. The inherent properties associated with nanoscale structures such as high surface-to-volume ratio are expected to result in strong filler-matrix interfacial adhesion [21]. Silicon dioxide (SiO_2) nanoparticles stand out as a non-toxic and biocompatible inorganic filler with high hardness and toughness. In previous studies on conventionally manufactured PEEK-based composites, SiO_2 nanoparticles have exhibited promising enhancement of tensile properties, stiffness, thermal stability, and tribological performance [22–25]. In a recent study, Lin et al. [25] reported that the combination of 2 wt% SiO_2 in SCF-PEEK with melt-compounding and injection molding exhibited the optimum tribological properties. It was found that the presence of nano-SiO_2 enhances the formation of transfer layers to reduce friction and wear. In another study, the same authors investigated the influence of releasing nano-SiO_2 into the sliding contact interface to reduce friction and wear of 3D printed SCF-PEEK and steel [26]. The improvement of friction performance was attributed to the rolling of nano-SiO_2 in the contact interface and the reduction of adhesion between the tribo-pairs by releasing rigid nanoparticles into the tribo-system. This approach points out the ability of nano-SiO_2 to enhance the self-lubricating ability of 3D printed PEEK composites. Recently, Lv et al. [20] proposed a multi-material composite structure prepared by FFF with alternating layers of SiO_2-PEEK and SCF-PEEK. The results offer remarkable reinforcement effects of nanoparticles and enhanced tribology of SCF-PEEK composites in FFF 3D printing with a novel material design.

Although extensive literature exists on the 3D printing of PEEK, limited attention has been given to the nanoparticle-reinforced PEEK composites for FFF3D printing. Based on the discussed literature, SiO_2 can be an ideal candidate to improve the structural properties of 3D printed SCF-PEEK. The primary aim of this study is to enhance the processing of nano-SiO_2 reinforced SCF-PEEK composites for FFF 3D printing. Multiscale composite filaments were produced in-house as feedstock for 3D printing via melt-extrusion. The extruded composite filaments and 3D printed components were examined for microstructure and thermo-mechanical properties, with a special emphasis on the effect of nano-SiO_2 on the properties of SCF-PEEK. It is expected that the outcome of this presented research work will enhance the understanding of the property-enhancing effect of nanoscale SiO_2 and microscale SCF in FFF 3D printing of PEEK composites.

2. Experimental details

2.1. Materials

PEEK 450 PF fine powders were purchased from Victrex™ (Lancashire, UK) with an average size of 50 μm, 1300 kg/m^3 density, and 350 Pa s melt viscosity at 400 °C. Milled SCFs (Tenax-A HT M100 100mu, Teijin Carbon) with an average length and diameter of 100 and 7 μm, respectively, and a density of 1820 kg/m^3 were used as microscale fillers. Silicon dioxide (SiO_2) nanoparticles (CAS Number 7631-86-9, Sigma-Aldrich, Sweden) were used with an average size of 10–20 nm and a density of 2200–2600 kg/m^3.

2.2. Filament extrusion

The composition of PEEK powders and micro/nano-fillers used for the filament extrusion are listed in Table 1. Composite filaments were obtained in a two-step procedure: wet mixing to prepare the composite powders and melt-compounding to extrude the filaments. Composite powders required for the extrusion process were prepared in multiple batches of 30 g to ensure adequate distribution and dispersion of fillers into the polymer matrix. An overview of the stepwise preparation of composite powders followed by filament fabrication is illustrated in Fig. 1.

Initially, PEEK powders were dried overnight in an air-circulating oven at 120 °C to ensure the elimination of residual moisture before mixing with fillers. To prepare the multiscale composite filaments, SiO_2 nanoparticles were first dispersed in ethanol by tip sonication for 1 h. Pre-dried PEEK powders were then added to nanoparticle dispersion followed by tip sonication for another 1 h. Next, SCFs were added to the SiO_2-PEEK mixture and dispersed in an ultrasonic bath for 30 min. Later, SiO_2-SCF-PEEK suspension was further mixed by magnetic stirring for 24 h. The suspension was then oven-dried at 80 °C for 24 h to obtain the multiscale composite powders. The dried powders were extruded into filaments by melt compounding using a Process 11 parallel co-rotating twin-screw extruder with an L:D ratio of 40, 11 mm screw diameter, and 2.0 mm die diameter (Thermo Scientific, Germany). The screw rotation speed was set to 200 rpm and temperatures ranging from 370 to 390 °C were used. The temperature profile for each heating zone during melt compounding is presented in Fig. 1. The extruded filaments were air-cooled and spooled under tension to obtain continuous filaments with an average diameter of ~1.75 ± 0.05 mm. Neat PEEK and SCF-PEEK filaments were also extruded using the same compounding method for comparison.

2.3. Specimen fabrication

CreatBot PEEK-300 high-temperature FFF 3D printer (Henan Suwei, China) was used to fabricate rectangular specimens with a dimension of 30 × 15 × 3 mm^3. Autodesk Fusion 360 (California, USA) was used to prepare the 3D CAD models (STL format) required for layer slicing. A printable G-code file with desired slicing and process parameters was created using Simplify3D V5 (Cincinnati, USA). Table 2 lists the detailed process parameters used for the fabrication of testing specimens [9]. The extruded filaments were oven-dried at 120 °C for 12 h before printing to remove the moisture. The printing chamber was pre-heated for nearly 15–20 min prior to individual printing to reduce the temperature gradient. The composite filaments were printed after cleaning the nozzle to avoid potential clogging in the presence of rigid fillers.

2.4. Scanning electron microscopy (SEM)

The dispersion quality and microstructure of the raw materials and composite powders were investigated using an FEI Magellan 400 extreme high-resolution scanning electron microscope (XHR-SEM, FEI Company, USA). The purpose of XHR-SEM was to determine the

Table 1
Composition of PEEK powders and fillers used.

Designation	Compositions [wt%]		
	PEEK	Micro-SCF	Nano-SiO_2
Neat PEEK	100	–	–
SCF-PEEK	90	10	–
SiO_2-SCF-PEEK	88	10	2

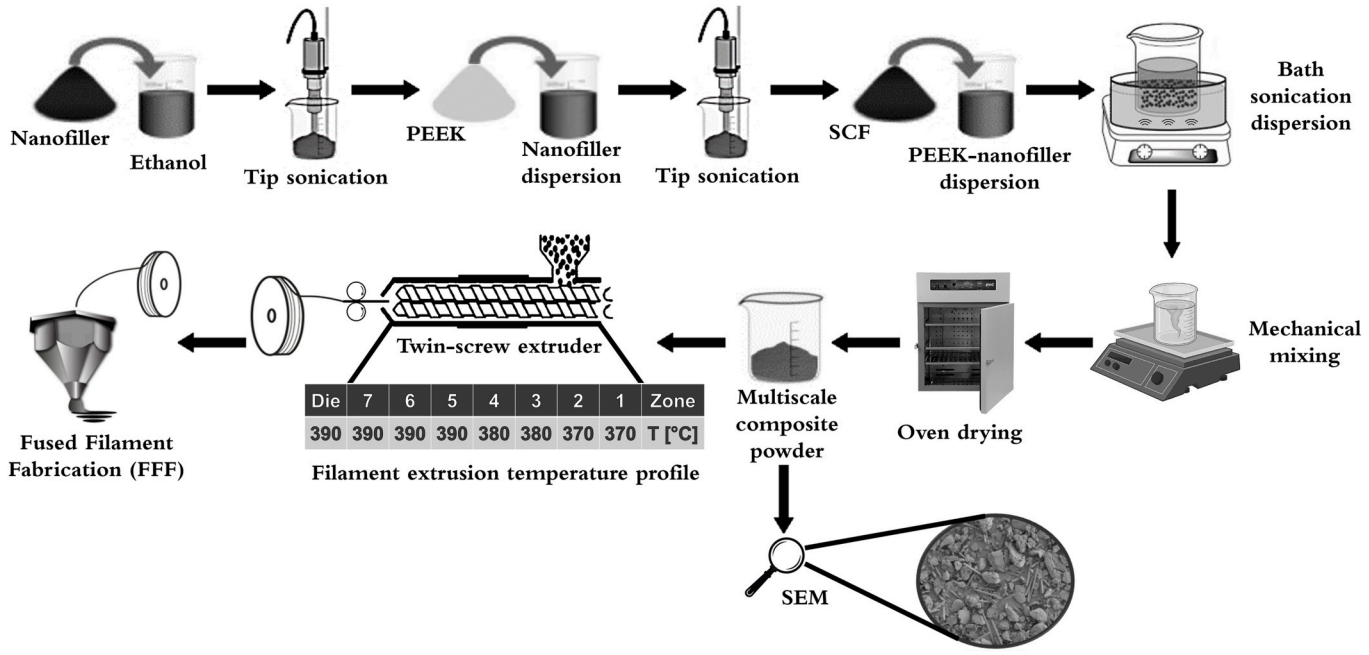

Fig. 1. Overview of the manufacturing process.

Table 2
Fused Filament Fabrication (FFF) printing conditions.

Process parameters	Values
Raster angle [deg]	+ 45°/-45°
Printing speed [mm/s]	50
Printing nozzle temperature [°C]	440
Build platform temperature [°C]	140
Build chamber temperature [°C]	120
Extruder nozzle diameter [mm]	0.40
Layer thickness [mm]	0.10
Infill density [%]	100
Infill pattern	Rectilinear
Build orientation	Horizontal

morphology of matrices and fillers prior to the compounding process. Also, the microstructure analysis of the fractured surfaces of extruded filaments and printed parts was carried out using XHR-SEM and a JSM-IT300 SEM (JEOL, Peabody, USA) equipped with energy dispersive X-ray spectroscopy (EDX). Before SEM analysis, a 15 nm platinum layer was sputter coated on the specimens.

2.5. Porosity analysis

The immersion method according to ASTM D792 [27] was used to measure the apparent densities (M_d) of extruded filaments and 3D printed polymers. Three repeated mass measurements were taken for reliable data. The density of water used to immerse the specimen during wet mass measurements was 997.8 kg/m^3 at 22 °C. The volumetric porosity or void content (V) was calculated based on ASTM D2734 [28]. Theoretical densities (T_d) of PEEK composites were calculated based on their degree of crystallinity (X_C) obtained from the heating scan of DSC analysis (see Ref. [9] for more details). A fully amorphous PEEK density of 1263 kg/m^3 and a fully crystalline PEEK density of 1400 kg/m^3 were used to apply the rule of phases [29]. The theoretical densities of 1820 and 2200 kg/m^3 were used for SCF and SiO_2, respectively as specified by the supplier's technical datasheet. In addition, a digital image processing software Dragonfly 3D World (Version 2024, Object Research Systems, Montreal, Canada) was used to quantify the void contents from the 2D SEM micrographs. The porosity analysis was performed after the pore segmentation on fractured surfaces of filaments and printed parts.

2.6. X-ray micro-computed tomography (XMT)

X-ray micro-computed tomography (XMT) was used to investigate the distribution of fillers and internal irregularities in the printed composites with a Zeiss Xradia 620 Versa (Carl Zeiss Company, Pleasanton, USA). Tomography scans were conducted at an acceleration voltage of 50 kV, 4.5 W source power, 20× magnification, 1.0 mm field of view, and 0.5 μm voxel size. 3601 projections were acquired with an exposure time of 7 s per scan, and the total scan time was 8.5 h. Dragonfly 3D World software was used to obtain the visualizations and porosity analysis from XMT scans. A detailed pore segmentation workflow can be found elsewhere in our previous work [30].

2.7. Thermal characterization

Differential scanning calorimetry (DSC3+, Mettler Toledo) was used to determine the thermal transition parameters of extruded filaments and printed parts. Samples weighing about 8–10 mg were heated from 25 to 450 °C and cooled to 25 °C in a nitrogen atmosphere with the heating and cooling rates of 10 °C/min. The glass transition temperature (T_g), melting peak temperature (T_m), crystallization peak temperature (T_c), and degree of crystallinity (X_C) were recorded. X_C was calculated from the heating scans using Eq. (1) [31],

$$X_C = \frac{\Delta H_m}{(1-w)\,\Delta H_m^0} \text{ x } 100\% \quad (1)$$

where, ΔH_m is the measured melting enthalpy, w is the weight fraction of fillers, and ΔH_m^0 is the theoretical melting enthalpy corresponding to a 100 % crystalline PEEK (130 J/g [29]).

Thermogravimetric analysis (TGA/DSC3+, Mettler Toledo) was performed to investigate the thermal stability of extruded filaments and printed parts in a nitrogen atmosphere. Samples weighing about 8–10 mg were heated from 25 to 800 °C at a heating rate of 5 °C/min in alumina crucibles. The average values of three measurements are reported.

2.8. X-ray diffraction (XRD) analysis

X-ray diffraction (XRD) analysis was performed to investigate the crystalline structure of 3D printed parts using a PANalytical Empyrean X-ray diffractometer (Malvern, UK). XRD patterns were recorded with a 1.8 kW Cu-Kα X-ray source of 1.5406 Å wavelength (λ). A PIXcel-3D detector operating at 40 kV and 40 mA in 2θ range of 5° to 70° was used with a scanning rate of 5°/min at room temperature in air. A quantitative analysis of the degree of crystallinity (X_C^*) was obtained by a deconvolution of the crystalline and amorphous parts of the diffractogram using the Gaussian function in OriginPro 2023b (Origin Lab, USA). After deconvolution, X_C^* was calculated from the area under the crystalline peaks (A_c) and amorphous halo (A_a) using Eq. (2) [32],

$$X_C^* = \frac{A_c}{A_c + A_a} \text{x } 100\% \tag{2}$$

Furthermore, the average interplanar distance between atoms (d-spacing) and mean crystallite size were obtained based on Bragg's Law using Eq. (3) and Scherrer equation using Eq. (4) [33], respectively.

$$d_{hkl} = \frac{\lambda}{2 \sin \theta} \tag{3}$$

where, d_{hkl} is the d-spacing corresponding to the plane positions i.e. Miller indices (h k l), λ is X-ray wavelength, and 2θ is Bragg's angle in radians.

$$D_{hkl} = \frac{K \lambda}{\beta \cos \theta} \tag{4}$$

where, D_{hkl} is the mean crystalline size, K is the shape factor (Scherrer constant, taken as 0.94 for spherical crystals), and β is full width at half maximum intensity (FWHM) in radians corresponding to the plane positions (h k l).

2.9. Dynamic mechanical analysis (DMA)

Dynamic mechanical analysis (DMA 850, TA Instruments) was employed to investigate the influence of filament fillers on the viscoelastic behavior of 3D printed PEEK. All tests were conducted with a specimen dimension of 30 × 15 × 3 mm^3 in a temperature sweep mode ranging from 25 to 250 °C with a heating rate of 3 °C/min at 1 Hz frequency and 20 μm amplitude using a single cantilever configuration.

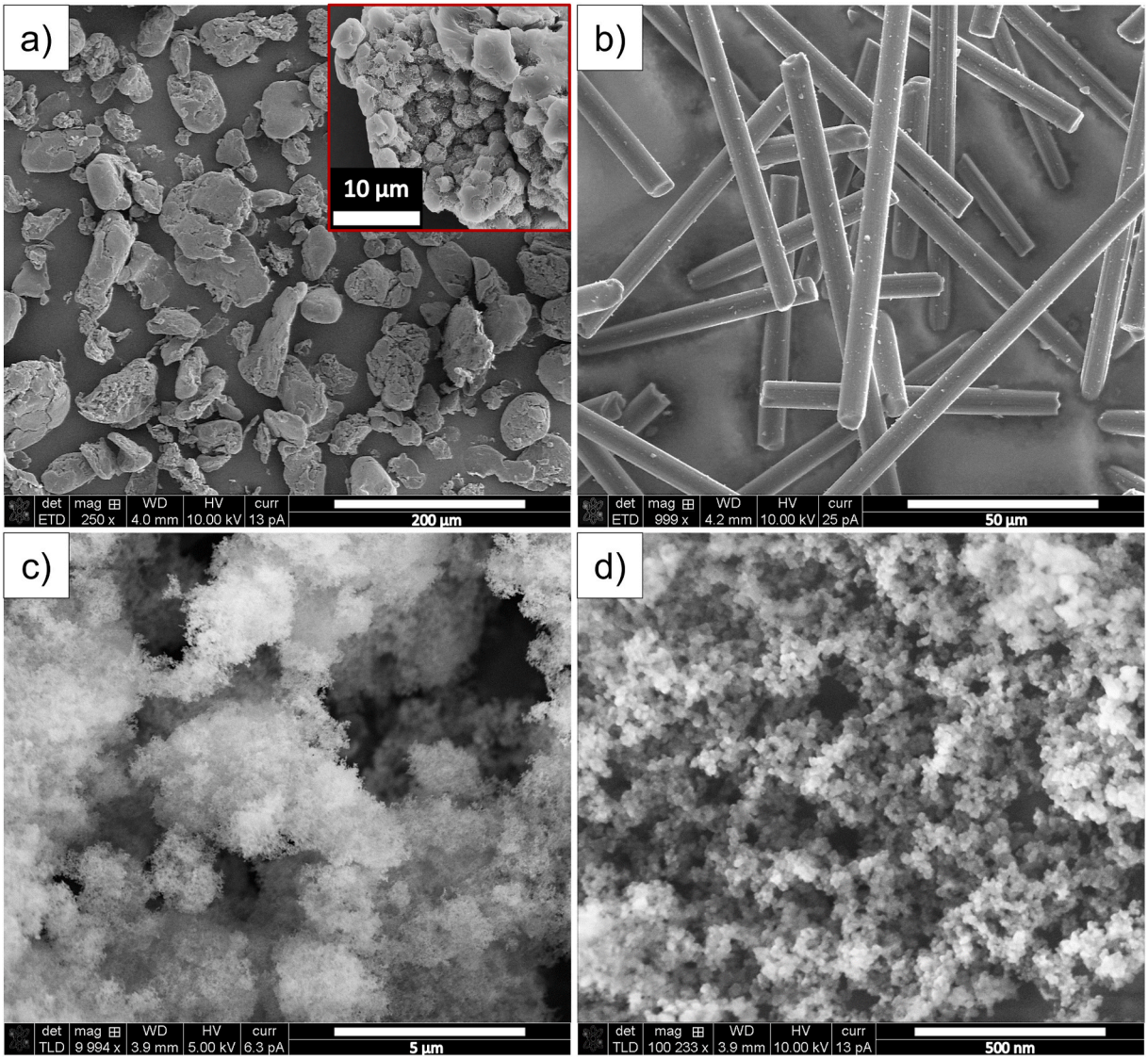

Fig. 2. Representative SEM images of as-received polymer powders and fillers: (a) neat PEEK, (b) short carbon fibers, and (c, d) SiO_2 nanoparticles.

3. Results and discussion

3.1. Microstructure morphology

Fig. 2 shows representative morphologies of as-received PEEK powders, short carbon fibers, and SiO_2 nanoparticles used. The dispersibility and compatibility of reinforcing fillers with polymer matrix determine the processing quality of filaments and consolidated composites. Therefore, the dispersion quality of SiO_2 and SCF in the PEEK matrix was assessed before and after the filament extrusion. Fig. 3 shows the morphology of SiO_2-SCF-PEEK composite powders before the melt-compounding process. A uniform distribution of fibers can be observed with the polymer resin in Fig. 3(a). XHR-SEM images exhibited good dispersibility of SiO_2 particles in the PEEK matrix, Fig. 3(c and d). The clustering tendency of SiO_2 forming nanoparticle aggregates in the PEEK matrix was realized, marked with red arrows in Fig. 3(d). SiO_2 nanoparticles adhered to the SCF surfaces were also observed, marked with red circles and arrows in Fig. 3(b).

PEEK-based composite filaments were successfully fabricated using wet mixing and melt compounding methods. Fractured surfaces of composite filaments after extrusion showed randomly distributed fibers and voids, Fig. 4. The fibers were preferentially aligned along the extrusion direction due to the flow. The majority of voids present on the filament cross-section occurred during the fracture, as a result of fiber pull-out from the matrix. Recent studies on the in-house extrusion of SCF-PEEK filaments have reported the existence of voids, which consequently resulted in the reduction of mechanical properties of printed parts [8,34]. However, no obvious fiber-matrix interfacial gaps were observed for both composite filaments in the present study. The presence of wetted fibers in polymer resin exhibits adequate interfacial bonding and adhesion for multiscale filaments, Fig. 4(b2). Moreover, relatively rougher fiber surfaces of multiscale filaments demonstrate better adhesion to the matrix compared to SCF-PEEK filaments, see insets of Fig. 4(a2, b2). Such topography is likely to enhance the mechanical interlocking, further improving the interfacial adhesion between the PEEK matrix and fibers during the 3D printing process. Additionally, EDX analysis of multiscale composite filaments confirmed the presence of SiO_2 on the fractured surfaces indicating good dispersibility, Fig. 5.

Fig. 6 presents the fractured surfaces of 3D printed composites under tensile stress along the longitudinal direction with respect to the raster angle orientation. Fractography demonstrated matrix fracture and

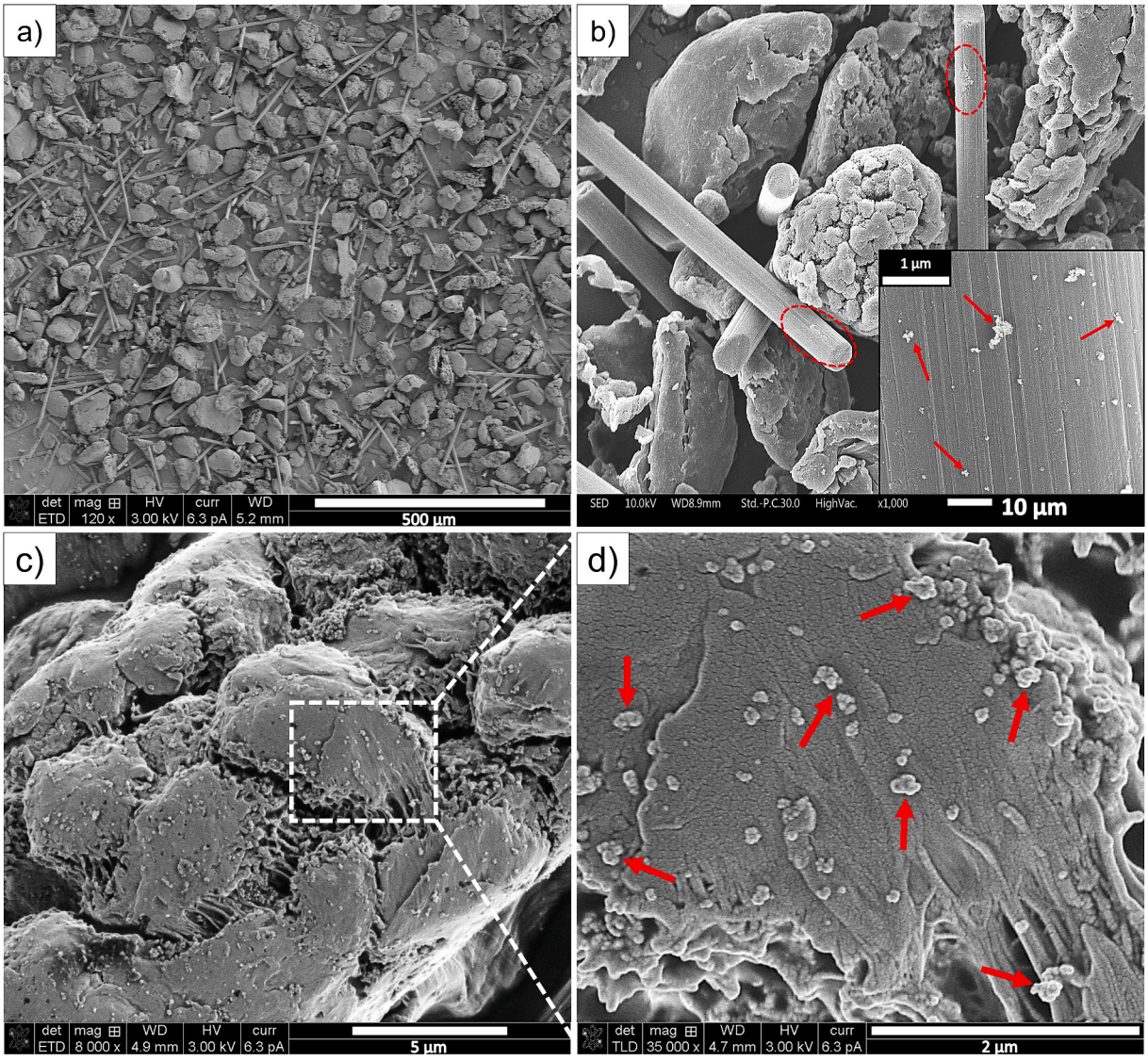

Fig. 3. Microstructure morphology of multiscale composite powders showing the presence of SiO_2 and SCF in PEEK: (a) overview indicating the distribution of polymer resin and fillers (b) SiO_2 adhered on the SCF surfaces (c, d) SiO_2 dispersed in the polymer resin.

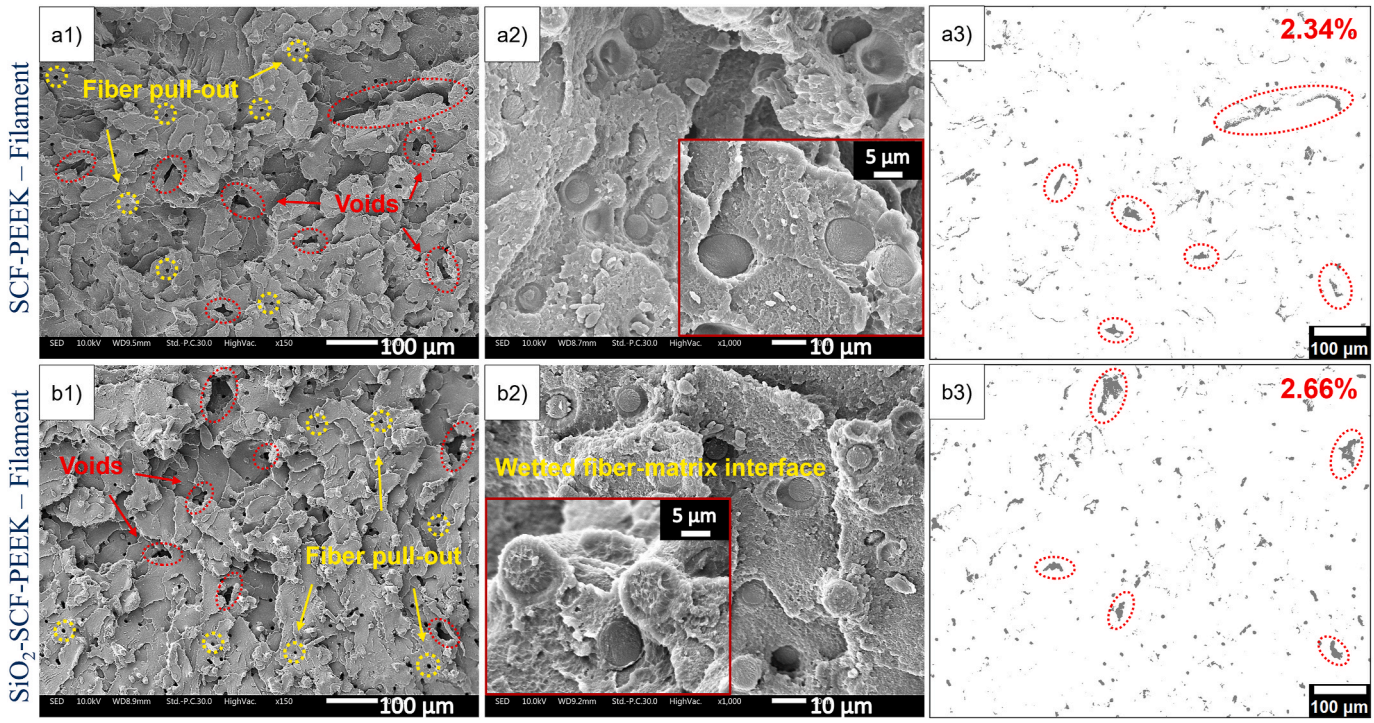

Fig. 4. Fractured surfaces of extruded composite filaments: (a1, a2) SCF-PEEK and (b1, b2) SiO_2-SCF-PEEK; (a3, b3) quantification of internal defects on fractured surfaces using 2D image processing based on SEM micrographs (a1) for SCF-PEEK and (b1) for SiO_2-SCF-PEEK (white represents the bulk material and gray represents the internal voids and irregularities from the fracture).

rupture of layers indicating brittle fracture as the predominant failure mechanism. The morphologies of printed composites showed a uniform distribution of fibers, analogous to the extruded filaments, Fig. 4(a1, b1) versus Fig. 6(a1, b1). The presence of visible layer boundaries were present for both printed composites, indicative of interlayer gaps resulting from the lack of fusion defects. Meanwhile, 3D printed multiscale composites showed a relatively lower presence of fiber pull-out, intralayer voids, and irregularities originating from the fracture, compared to 3D printed SCF-PEEK. This indicates that the printing process further improved the fiber-matrix bonding in the presence of nanoparticles. Besides, well-wrapped fibers in the PEEK matrix revealed no obvious interfacial gaps, meaning a stronger filler-matrix adhesion which restricts the debonding during fracture in the presence of nano-SiO_2, Fig. 6(b2). The high surface energy of nano-SiO_2 improves the wetting of SCF by the PEEK matrix, promoting interfacial adhesion, similar to the observation for multiscale filaments in Fig. 4(b2). Also, the high surface-to-volume ratio of nano-SiO_2 enables strong interfacial bonds with the PEEK matrix. Therefore, the improvement in fiber-matrix bonding and interfacial adhesion can be attributed to the combination of mechanical interlocking and surface energy effects of nanoparticles. It has been reported that this tendency is highly accentuated at lower loadings of nanoparticles (usually less than 5 wt%), as it ensures appropriate dispersion and homogeneity [21]. Nonetheless, XHR-SEM of printed SiO_2-SCF-PEEK composites revealed localized clustering of nanoparticles, forming small agglomerates spread on the SCF surfaces, see inset of Fig. 6(b2).

Finally, it is pointed out that in-house extrusion of neat PEEK filaments and 3D printed neat PEEK showed no significant differences in the fracture surface morphology compared to our previous study on commercial filaments [9]. On the contrary, composite filaments and corresponding printed parts resulted in reduced interfacial voids and internal irregularities. This improvement with fewer processing defects is expected to enhance the comprehensive properties and integrity of 3D printed materials. Additional microstructural analysis to understand the distribution of fillers and internal defects is discussed later.

3.2. Porosity analysis

Table 3 presents the measured apparent density and void content of extruded filaments and printed parts by immersion method. The extrusion process yielded composite filaments with internal porosity closer to the neat PEEK filaments. The comparable porosity for SCF-PEEK and SiO_2-SCF-PEEK filaments concur with the SEM observations with no substantial differences, Fig. 4. However, a higher degree of porosity was observed for the printed composites compared to neat PEEK. The reduced densities of printed composites with increasing volumetric porosity confirm the existence of increased internal defects compared to corresponding filaments. The inadequate interlayer and interfacial bonding generally introduce gaps around the adhesion points during layer-on-layer fabrication, acting as voids. Excitingly, the inclusion of nanoparticles reduced the porosity of 3D printed SCF-PEEK, hinting at the improved filler-matrix interface of the printed multiscale composites. Nanoscale reinforcing fillers are known to facilitate adhesion at the polymer interface, reducing the interfacial gaps between the microscale SCF and PEEK matrix [21]. Furthermore, the presence of nanoparticles in the SCF-PEEK interface improves the localized heat distribution during the deposition process. Consequently, a lower thermal gradient improves the printability and increases the interfacial bonding [31]. This could be the plausible reason for the reduced porosity of the printed multiscale composites compared to SCF-PEEK. It is further supported by the improved microstructure morphology for printed SiO_2-SCF-PEEK, discussed earlier in section 3.1. The higher void contents measured for printed composites compared to the filaments are the consequence of the printing process alone. Generally, FFF 3D printing produces inevitable interlayer and inter-bead gaps, primarily contributing to the increased porosity of printed parts compared to corresponding filaments [8,35]. Furthermore, the morphological observation and void content of SCF-PEEK filaments and printed parts in this study show substantial improvement compared to previous studies [8,9,34,35].

In addition, similar observations were collated from the internal porosity analysis based on 2D image processing of fractured surfaces

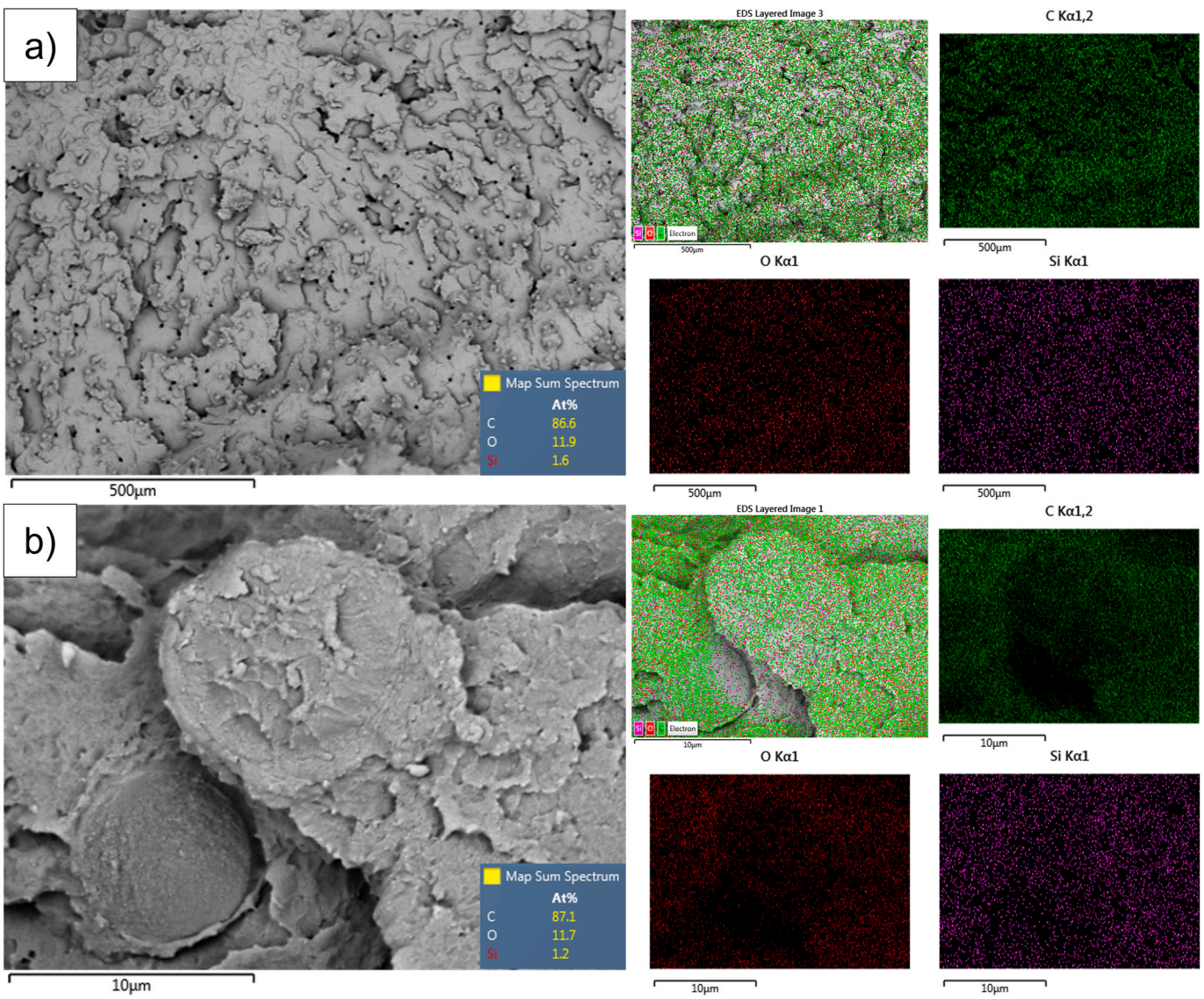

Fig. 5. EDX elemental mapping of multiscale composite filaments: (a) overview of the filament cross-section and (b) magnification showing the fibers in polymer matrix.

using Dragonfly software, Fig. 4(a3, b3) and Fig. 6(a3, b3). The segmentation process was performed based on the contrast differences in the SEM imaging data. The white region represents the bulk material (matrix and fillers), while the gray region represents the internal irregularities. The voids due to fiber pull-out are distributed throughout the analyzed surfaces of extruded filaments, evident as round dots after the pore segmentation, Fig. 4(a3, b3). The formation of interlayer gaps due to the separation of distinct layer boundaries on 3D printed composites is visible in Fig. 6(a3, b3). The volumetric porosity obtained from the image processing is around 2.34 % and 2.66 % for extruded SCF-PEEK and SiO_2-SCF-PEEK filaments, while it is 5.74 % and 3.85 % for their corresponding printed parts, respectively. However, this analysis technique is limited to the surface level and includes the defects formed during the fracture, such as fiber pull-out voids and layer breakage during the fracture. Therefore, an overestimation of the pore volume fractions could be observed as it is difficult to distinguish between the irregularities originating from the fabrication process and the fracture mechanism. On that note, additional microstructure analysis of internal morphology coupled with 3D visualization would facilitate more information regarding internal morphology.

3.3. X-ray micro-computed tomography (XMT)

XMT was used to qualitatively analyze the localized formation of porosity and distribution of fillers in the printed composites. Fig. 7 shows a representative 3D visualization of the internal morphology of printed SiO_2-SCF-PEEK after phase segmentation. In Fig. 7, XZ and YZ planes are perpendicular and parallel to the print bed, respectively. The distribution of fibers on the individual layers can be recognized in Fig. 7 (b). The accumulation of voids at the boundaries of adjacent layers resulted in the larger connected porosity due to the lack of fusion, Fig. 7 (c). The localized presence and morphology of fillers and internal defects were comparable for both printed composites, SCF-PEEK and SiO_2-SCF-PEEK.

The detailed microstructural analysis was performed after a 3-phase segmentation (matrix, fillers, and air) using grayscale thresholding (Otsu's method). The matrix, fillers, and internal pores are distinguished from the phase contrast due to the differences in their density, illustrated in Fig. 8. The polymer matrix is denoted by the dark contrast region, fibers are represented by highly pronounced white entities and red signifies the internal pores. The distribution of fibers exhibited a high degree of uniformity for both composites, presented in Fig. 9(b–d). On

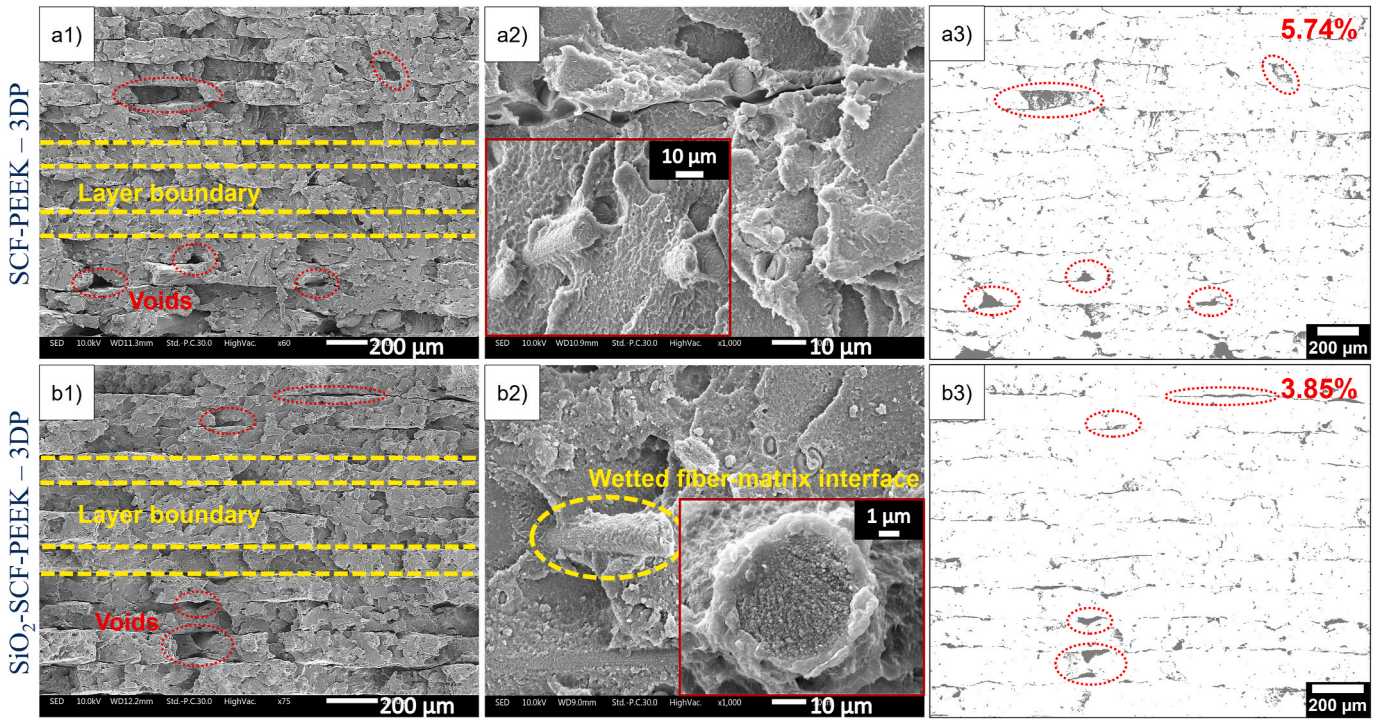

Fig. 6. Fractured surfaces of 3D printed composites: (a1, a2) SCF-PEEK and (b1, b2) SiO_2-SCF-PEEK; (a3, b3) quantification of internal defects on fractured surfaces using 2D image processing based on SEM micrographs (a1) for SCF-PEEK and (b1) for SiO_2-SCF-PEEK (white represents the bulk material and gray represents the internal voids and irregularities from the fracture).

Table 3
Apparent density and calculated void content using the immersion method.

Designation	Calculated theoretical density, T_d [kg/m^3]	Apparent density, M_d [kg/m^3]		Void content, V [%]	
		Filaments	Printed	Filaments	Printed
Neat PEEK	1307	1283 ± 1.7	1282 ± 1.8	1.7 ± 0.1	1.9 ± 0.1
SCF-PEEK	1343	1314 ± 4.2	1273 ± 6.3	2.2 ± 0.3	5.2 ± 0.5
SiO_2-SCF-PEEK	1355	1327 ± 1.1	1316 ± 3.7	2.1 ± 0.1	2.9 ± 0.3

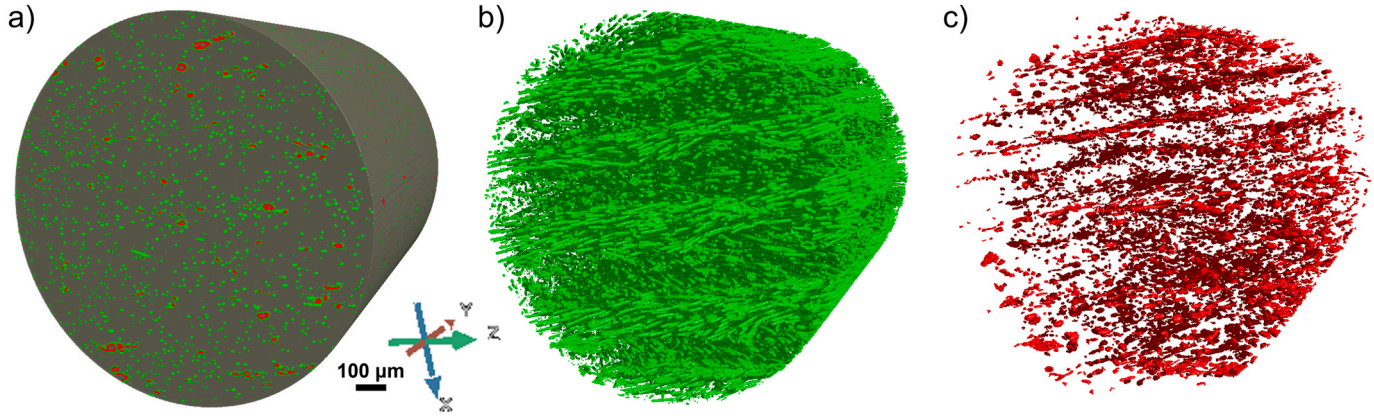

Fig. 7. Representative 3D visualizations from tomography phase segmentation of printed multiscale composite: (a) segmented region of interest (ROI) including matrix (dark green), fibers (light green), and pores (red), (b) segmented ROI with fibers, and (c) segmented ROI with internal porosity. (For interpretation of the references to colour in this figure legend, the reader is referred to the Web version of this article.)

the contrary, the formation and distribution of pores seemed to lack homogeneity. This was true for both printed composites presented in this study, see Fig. 9. Additionally, distinct morphological features among the porosity contents were detected along the different slices. A strong presence of spherical voids and several elongated bead-shaped voids were observed, Fig. 9(a–c).

For quantitative analysis, the calculation of porosity was performed with a minimal threshold of 9 voxel counts within the representative volume of 1000 × 1000 × 1000 µm^3. The localized pore volume fractions of 1.03 % and 0.9 % were obtained for SCF-PEEK and SiO_2-SCF-

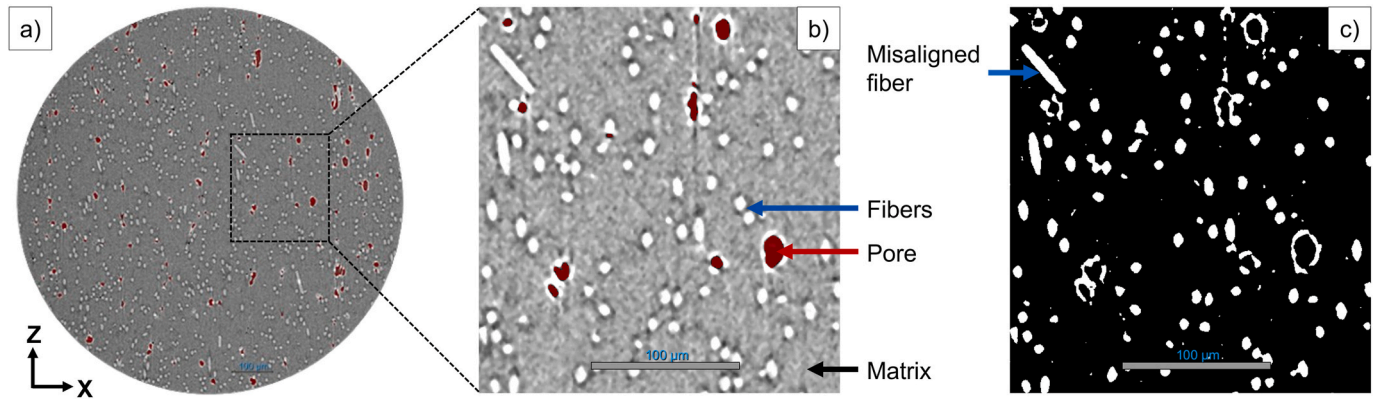

Fig. 8. Representative 2D slice of SiO_2-SCF-PEEK after phase segmentation along XZ plane of tomography scans perpendicular to print bed: (a) overview of the entire scanned region, (b) segmentation showing polymer matrix, fillers, and pores (c) filler distribution extracted from 2D slice.

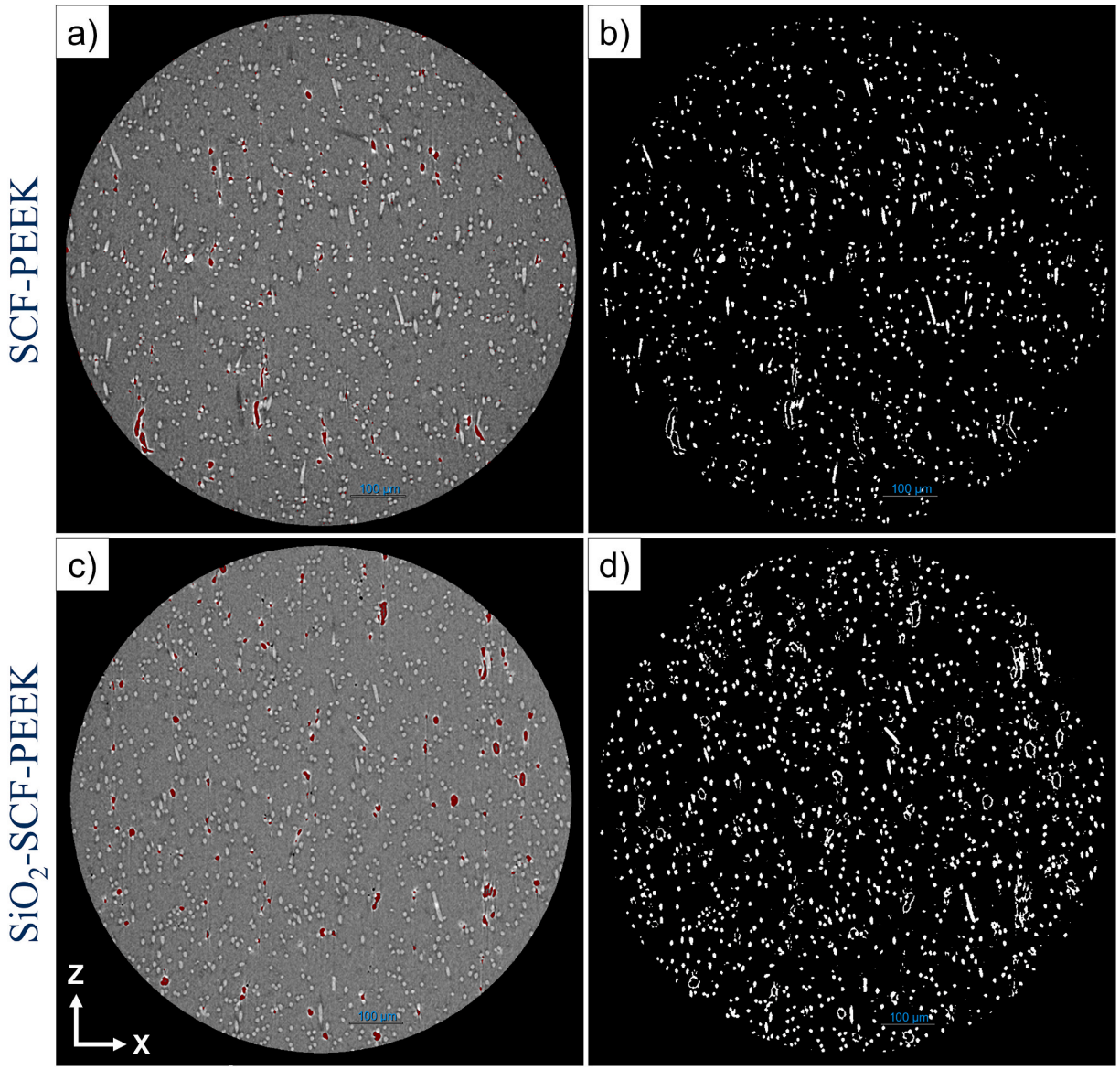

Fig. 9. Representative 2D slices of composites after phase segmentation along XZ plane of tomography scans perpendicular to print bed: (a, b) SCF-PEEK and (c, d) SiO_2-SCF-PEEK; distribution of fibers extracted from the corresponding 2D slices of (b) SCF-PEEK and (c) SiO_2-SCF-PEEK.

PEEK, respectively. The volumetric porosity estimated using XMT in this study is similar to Rodzeń et al. [5] for 30 wt% SCF reinforced PEEK (1.0–2.3 %), while it is lower than the porosity contents reported in Refs. [12,15]. The majority of pore volume fraction (>94 %) was contributed by the spherical voids less than 1000 μm^3. The presence of nanoparticles appears to have no obvious influence on the distribution of internal defects within the scanned region.

Furthermore, fiber analysis was carried out using the Open Fiber Segmentation tool available in Dragonfly 3D World developed by Sosa-Rey et al. [36] for short fiber reinforced composites. A new region of interest (300 × 300 × 300 μm^3) was selected from a previously segmented ROI containing fibers, as shown in Fig. 10. A smaller ROI was applied to reduce the dataset due to the limited computational capability. Fiber identification within the analyzed region resulted in fiber volume fractions of 8.91 % and 9.23 % for SCF-PEEK and SiO_2-SCF--PEEK, respectively. For both composites, the stacking of fibers on individual layers was visible, as illustrated in Fig. 10(b). The fibers in individual layers were mostly oriented along the deposited strategy (+45°/-45°) parallel to the print bed (YZ plane). The computed measurements revealed that the average length of fibers reduced to a range of 25–50 μm, against the original average length of 100 μm. This shows that the shear-induced interaction during melt-compounding shortens the fiber length.

3.4. Thermal characterization

Initially, thermal analysis of filaments was performed to determine the appropriate printing temperature range for extruded composites. The decomposition temperatures from TGA and melting temperatures from DSC were evaluated to confirm the upper limit (~545 °C) and lower limit (~345 °C) of the printing temperatures, respectively. TGA and DSC thermograms were further analyzed to investigate the thermal stability and thermal-transition parameters of 3D printed parts.

The thermal decomposition curves for the extruded filaments from TGA were analogous to their corresponding printed parts with insignificant differences, Fig. 11. This shows that the printing process had a marginal impact on the thermal stability of the PEEK matrix for all tested materials. As observed from the degradation onset temperatures (T_{onset}), the first decomposition step starts around 558 °C for neat PEEK. At this step, random chain scission of ether and ketone bonds starts with phenol being the primary decomposition product [3,37]. All materials experienced a rapid mass loss with the volatilization of around 40 % polymer mass just below 600 °C. In the second decomposition stage, slower volatilization of residue occurs resulting in carbonaceous char with over 50 % residue still present at 800 °C.

The inclusion of SCF slightly reduced the T_{onset} for both neat PEEK filaments and corresponding printed parts, Fig. 12(a). Similarly, the peak of the first derivative of TGA (DTGA) curves revealed that the temperature at maximum degradation (T_d) occurred earlier for SCF-PEEK compared to neat PEEK, Fig. 12(b). This implies that the thermal stability of the PEEK matrix was slightly reduced with the inclusion of 10 wt% SCF. On the contrary, incorporating 2 wt% SiO_2 nanoparticles in SCF-PEEK increased the T_{onset} and T_d, suggesting improved thermal stability of multiscale filaments and printed parts. In addition, a 5 % weight loss of extruded neat PEEK filaments occurred at a maximum of 560 °C. The curves of composite filaments shifted to the right showing 5 % weight loss for SCF-PEEK and SiO_2-SCF-PEEK at 562 °C and 563 °C, respectively, presented in Fig. 11(a1). This agrees with the increment of thermal decomposition temperatures registered for 2.5 wt% nano-SiO_2 filled PEEK [38]. The combined addition of micro-SCF and nano-SiO_2 in neat PEEK was effective in reducing the weight loss rate, demonstrating that the composites are relatively more stable at higher temperatures. It is further reflected by the temperatures at the end of linear weight loss for composites compared to neat PEEK, Fig. 11(a2).

Fig. 13(a, b) shows the heating and cooling scans of the DSC curves for extruded filaments and printed PEEK composites. It is clear from the similarity of heating scans that insignificant changes were recorded for T_m (340 ± 0.5 °C) for all tested specimens, presented in Fig. 14(a). The comparable T_g (152 ± 1 °C) of neat PEEK and composites were registered for extruded filaments and corresponding printed parts, Fig. 14(b). This indicates that the filament extrusion and 3D printing process did not reduce the chemical integrity of the PEEK matrix in the presence of nanoscale and/or microscale fillers.

X_C for composite filaments was slightly reduced, while an increasing

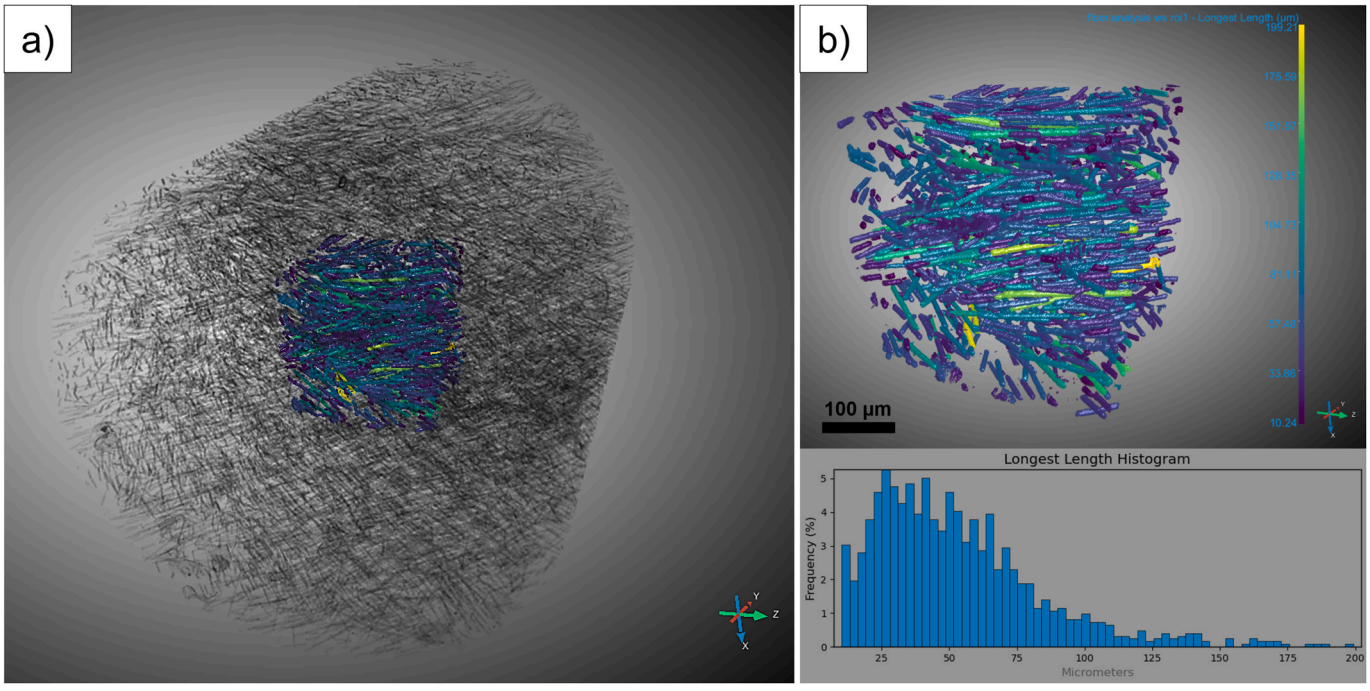

Fig. 10. Representative fiber segmentation of multiscale composite: (a) 3D visualization with a smaller ROI containing fibers and (b) analysis for the length of individual fibers.

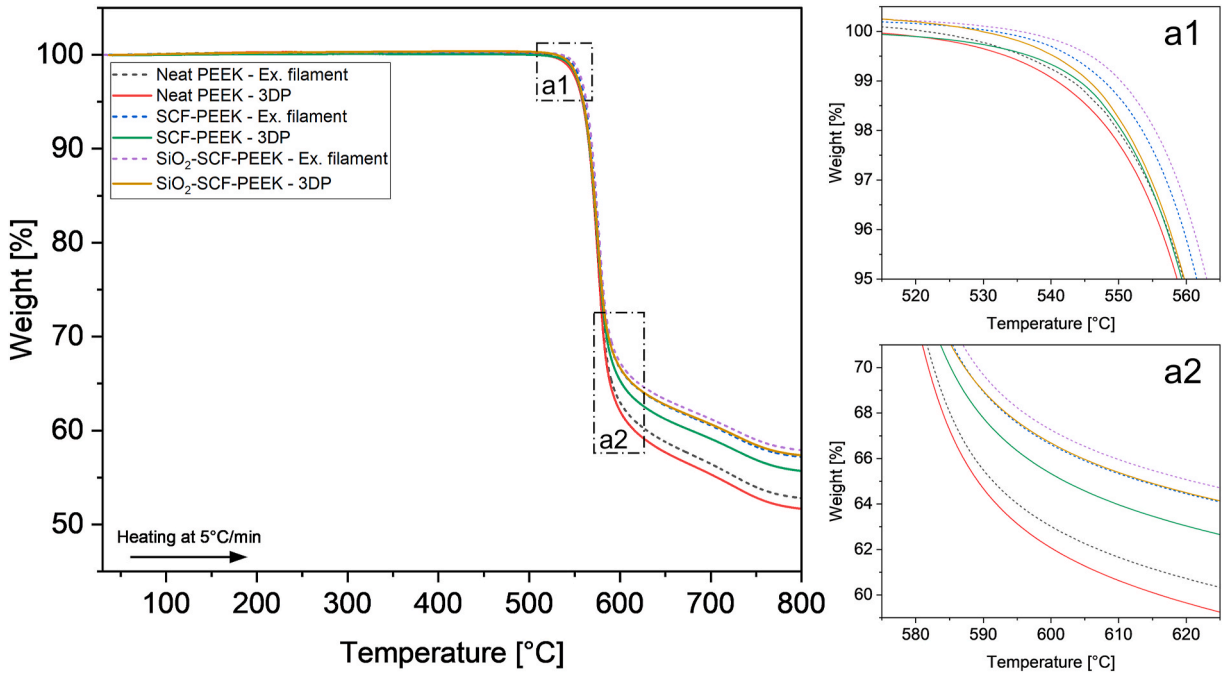

Fig. 11. Representative TGA curves of extruded filaments and printed parts: (a1) 5 % weight loss and (a2) end of linear weight loss.

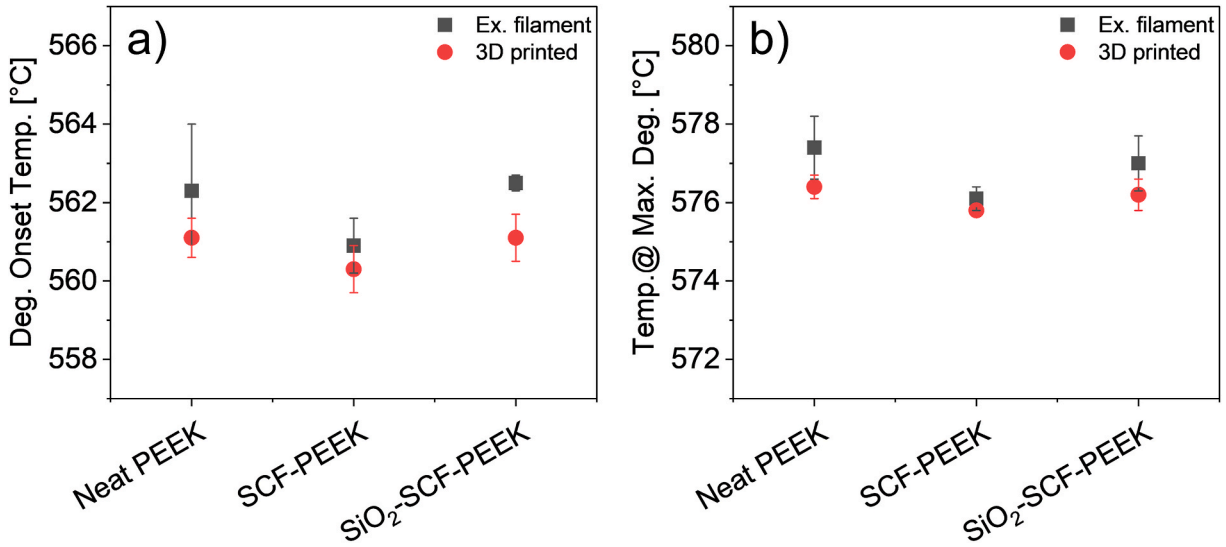

Fig. 12. (a) Degradation onset temperature (T_{onset}) and (b) temperature at maximum degradation (T_d) of extruded filaments and printed parts obtained from TGA.

trend was detected for printed composites compared to neat PEEK, Fig. 14(c). The maximum reduction in X_C value was 4.3 % for extruded multiscale filaments compared to neat PEEK filaments. The maximum increment in X_C value was 5.8 % for printed multiscale composites compared to printed neat PEEK. It should be noted that the crystallinity differences are not critical here, while the trend seems interesting. Similarly, X_C of 35 % for multiscale filaments increased to 42 % for their corresponding printed multiscale composites, demonstrating that the FFF process positively influenced the degree of crystallinity. The lower X_C for multiscale filaments can be attributed to a faster cooling process during the melt-extrusion. The presence of nanoparticles improves the interfacial heat dissipation, resulting in a relatively higher localized cooling rate compared to neat PEEK and SCF-PEEK filaments, leading to a noticeable decrease in the degree of crystallinity [31]. On the other hand, FFF process has a relatively lower thermal gradient and more homogeneous cooling process due to the heated chamber environment. During the printing process, the increased thermal conductivity of composite filaments in the presence of SCF results in a uniform heat distribution occurs along the adjacent layers [10]. This further minimizes the thermal gradient and the additional heat treatment under controlled temperature improves the crystallinity of printed composites. The re-melting of filaments and a slower cooling of deposited layers allow a higher degree of molecular chain mobility, enabling them to rearrange and recrystallize. Also, reorientation of the fibers might occur during this stage, possibly improving the microstructure of printed composites [5]. Meanwhile, a noteworthy increment of T_c was observed for printed composites (up to 8 °C) compared to printed neat PEEK, see Figs. 13(b) and 14(d). This suggests that less energy is required for the PEEK molecular chains to align at the interphase in the vicinity of nanoparticles. The incorporation of filament fillers and the printing process influenced the crystallization behavior of printed PEEK composites. These findings are in good agreement with the crystallization

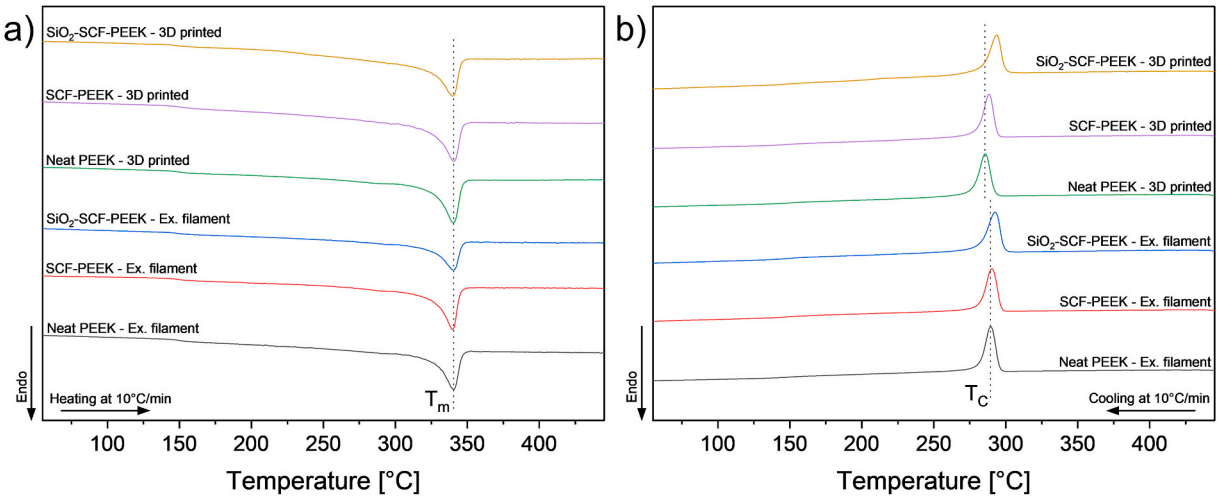

Fig. 13. Representative DSC curves of extruded filaments and printed parts: (a) heating scans and (b) cooling scans.

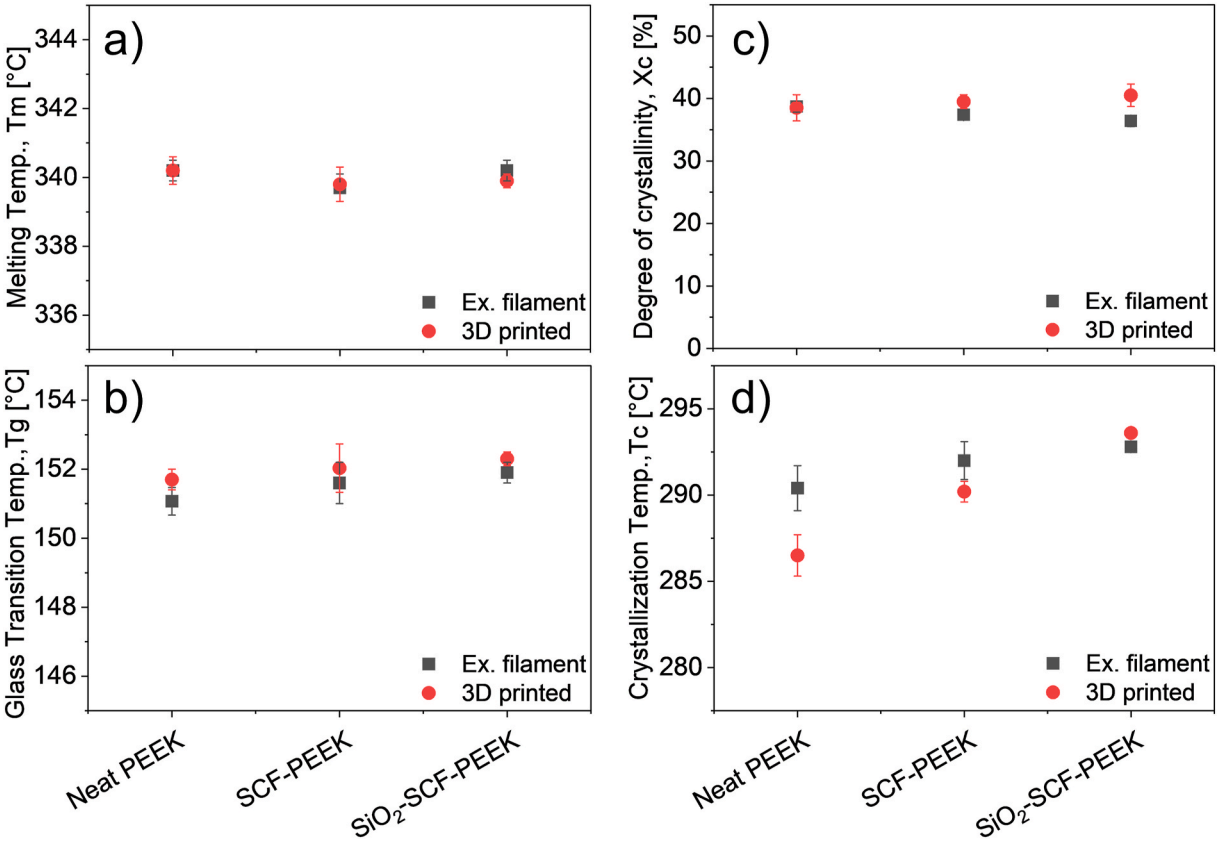

Fig. 14. (a) Melting temperature (T_m), (b) glass transition temperature (T_g), (c) degree of crystallinity (X_C), and (d) crystallization peak temperature (T_c) of extruded filaments and printed parts obtained from DSC.

behavior of nanoparticle-reinforced PEEK composites for FFF 3D printing in other studies [17,18].

3.5. X-ray diffraction (XRD) analysis

XRD patterns of 3D-printed neat PEEK, SCF-PEEK, and SiO_2-SCF-PEEK composites were investigated to obtain additional information on the crystalline characteristics, Fig. 15(a). All specimens exhibited the diffraction peaks associated with the orthorhombic unit cell of PEEK at 2θ angles of 18.7°, 20.7°, 22.6°, and 28.7° corresponding to (110), (111), (200), and (211) plane orientations, respectively [39]. XRD patterns of printed composites are qualitatively similar to that of neat PEEK, with no evidence of a distinct phase or shift in the angular positions. This signifies that the addition of micro-SCF and nano-SiO_2 does not affect the crystallographic orientation of the PEEK matrix.

Fig. 15(b) shows an example of the deconvolution of crystalline and amorphous parts from the diffractogram obtained for printed neat PEEK. The degree of crystallinity based on the deconvoluted diffractograms showed an increase with the addition of SCF and nano-SiO_2. 36 % X_C* for neat PEEK increased to 39 % and 47 % for SCF-PEEK and SiO_2-SCF-

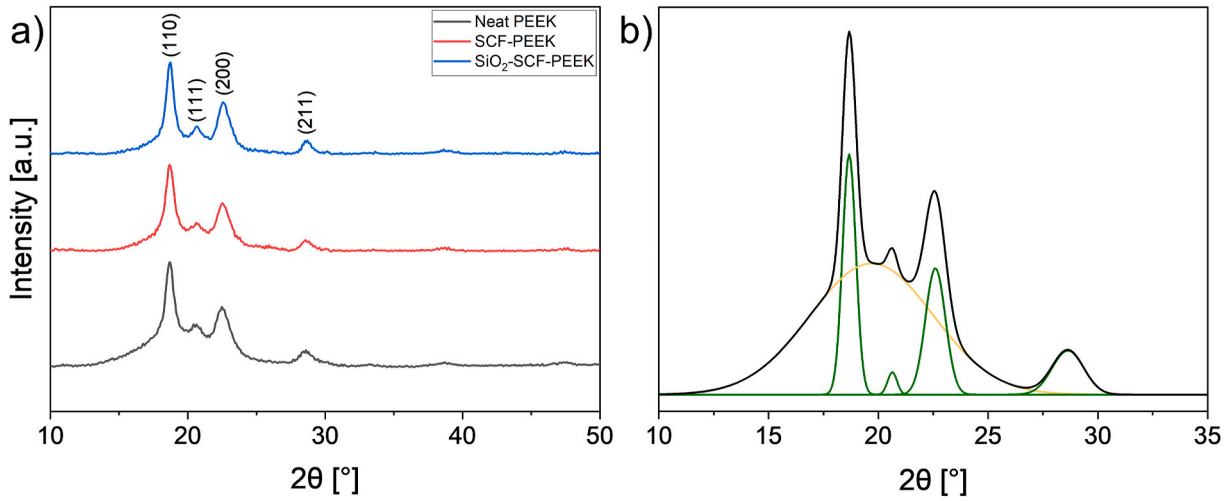

Fig. 15. (a) XRD patterns of 3D printed specimens and (b) representative deconvolution curves of crystalline and amorphous peaks for neat PEEK (green curves: crystalline parts, yellow curve: amorphous part). (For interpretation of the references to colour in this figure legend, the reader is referred to the Web version of this article.)

PEEK, respectively. As can be seen, the crystallinity values estimated using deconvoluted XRD patterns slightly differ from the DSC analysis, for instance, up to 6 % higher for printed multiscale composites. This can be attributed to the differences in measurement principle, calculation theory, and experimental setup behind the mentioned techniques. The estimation of the degree of crystallinity using the XRD corresponds to the crystalline lattice structures, considering both secondary and primary crystallites. On the other hand, the calculation of the degree of crystallinity using DSC involves measuring heat flow around the melting point and it mainly considers the melting enthalpy for primary crystallites and may not include the weaker secondary crystals which tend to melt in the region between T_g and T_m [5,40]. Nevertheless, the trend of increasing X_C of printed parts by the addition of SCF and nano-SiO_2 is consistent with both techniques.

The average interplanar distances (d-spacing, d_{hkl}) presented no relevant differences for printed neat PEEK (4.023 Å), SCF-PEEK (4.019 Å), and SiO_2-SCF-PEEK (4.016 Å). Meanwhile, the mean crystallite size (D_{hkl}) exhibited an increasing trend with the addition of SCF and nano-SiO_2, 10.4, 12.4, and 12.5 nm for neat PEEK, SCF-PEEK, and SiO_2-SCF-PEEK, respectively. The presence of SCF and SiO_2 could accelerate the crystal growth process, impacting the crystallographic structure of the PEEK matrix. Although the inter-atomic spacing is unaltered, the addition of SCF and nano-SiO_2 appears to influence the crystallite sizes in the 3D printing of PEEK. The increasing tendency of mean crystallite sizes (lamellar thickness) with varying contents and types of nanoparticles has been reported earlier for conventionally prepared PEEK nanocomposites [41]. The crystallization phenomena in this study support the filler-induced nucleating effect and thermal effects which increase the crystallization rate. This corroborates with the tendency of increasing T_c detected from DSC analysis in the presence of filament fillers in the PEEK matrix.

3.6. Thermo-mechanical analysis

Fig. 16 presents the storage modulus (E′), loss modulus (E"), and damping factor (tan δ) of 3D printed neat PEEK and composites. The storage modulus of neat PEEK increased with the addition of both microscale and nanoscale filament fillers. SCF-PEEK and SiO_2-SCF-PEEK exhibited up to 27 % and 40 % increments in E′ at 25 °C, respectively. This means that the incorporation of SCF and nano-SiO_2 remarkably increases the energy stored reversibly, improving the elastic response and stiffness of 3D printed composites. The addition of the SCF offers high mechanical strengths and load-bearing capacity, while nano-SiO_2 provides toughness and functions as a barrier to crack propagation. The combination of SCF and SiO_2 in the PEEK matrix enables the effective transfer of load to the reinforcement phases. Therefore, SiO_2-SCF-PEEK composites exhibiting the strongest E′ improvement is a consequence of nano-SiO_2-induced matrix-stiffening and interfacial reinforcement [23,

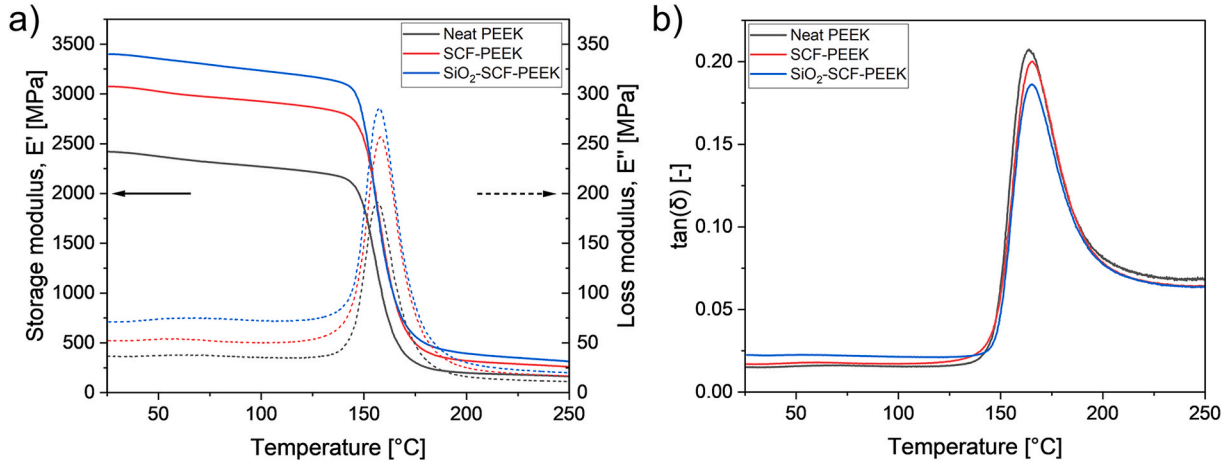

Fig. 16. Evolution of (a) storage modulus (E′) and loss modulus (E"), (b) damping factor (tan δ) as a function of temperature.

38]. The increased stiffness with the incorporation of SiO_2 nanoparticles can be beneficial to reduce the stress concentration on the fibers alone [42]. Similar enhancement effects of other nanoparticles on the dynamic mechanical properties of 3D printed PEEK have been reported earlier [18,19].

As can be observed in Fig. 16(a)–E' showed a progressive decline at increasing temperatures, with a sharp drop between 145 and 175 °C. This rapid drop in E′ means a higher degree of molecular free volume, enabling greater chain mobility and segmental motion at higher temperatures. Furthermore, the increase in loss modulus peaks for composites demonstrates enhanced energy dissipation potential in the presence of filament fillers. The cooperative improvement of dynamic moduli (E′ and E") for the multiscale composites at temperatures below and above T_g translates to stronger filler-matrix interfacial adhesion. The glass transition temperatures (T_g) were obtained from the peaks of loss modulus curves. There is an inconsequential difference in the T_g values for all the tested specimens, with T_g of around 157 °C. It is slightly higher than the T_g registered from DSC (~152 °C), but not unexpected, as DMA produces higher T_g values compared to the DSC technique [43].

The damping factor (tan δ) was reduced with the introduction of SCF and nano-SiO_2 in the PEEK matrix. The reduction in tan δ suggests that the composites are more elastic with a higher potential to store energy rather than dissipating. Besides, a lower tan δ peak for multiscale composite implies improved filler-matrix interaction and interfacial adhesion compared to SCF-PEEK. The nanoparticle distribution reduces the free volume and increases the interfacial area, restricting the segmental mobility around the nanoparticles [44]. It is beneficial for localized stress distribution at the filler-matrix interface, improving load transferability.

4. Conclusions

In this work, microscale SCF and SiO_2 nanoparticles were incorporated in the PEEK matrix to successfully fabricate multiscale composite filaments for FFF 3D printing. The effect of SiO_2 on the microstructure and thermo-mechanical properties of printed PEEK composites were discussed in detail. The incorporation of 2 wt% nano-SiO_2 greatly enhanced the fiber-matrix bonding and interfacial adhesion of 3D printed composites by mechanical interlocking and matrix-stiffening effects. Internal porosity of SiO_2-SCF-PEEK reduced to 2.9 % compared to 5.2 % for SCF-PEEK. Tomography revealed a uniform distribution of fibers on 3D printed PEEK composites, with the presence of internal defects. Thermal stability and crystallization behavior of printed SCF-PEEK were positively influenced by the presence of SiO_2 nanoparticles in SCF-PEEK. Additionally, FFF 3D printing process improved the degree of crystallinity of extruded multiscale filaments, 35 % X_C for SiO_2-SCF-PEEK filaments increased to 42 % X_C for their corresponding 3D printed parts. An increasing tendency of crystallization temperatures and mean crystal sizes were registered for 3D printed SiO_2-SCF-PEEK composites. T_C for SiO_2-SCF-PEEK increased to 294 °C from 290 to 286 °C for SCF-PEEK and neat PEEK, respectively. Similarly, the inclusion of SCF and SiO_2 increased the mean crystallite size to 12.5 nm compared to 10.4 nm for neat PEEK. The inclusion of SCF and SiO_2 improved the thermomechanical properties by significantly increasing the storage modulus up to 40 % compared to printed neat PEEK. Overall, the findings demonstrated a strong capability of nano-SiO_2 to improve the microstructure, thermal stability, and dynamic mechanical properties of 3D printed SCF-PEEK.

CRediT authorship contribution statement

Nayan Dhakal: Writing – original draft, Visualization, Validation, Methodology, Investigation, Formal analysis, Data curation, Conceptualization. **Cayetano Espejo:** Writing – review & editing, Supervision. **Ardian Morina:** Supervision. **Nazanin Emami:** Writing – review & editing, Validation, Supervision, Resources, Project administration, Funding acquisition, Conceptualization.

Declaration of competing interest

The authors declare that they have no known competing financial interests or personal relationships that could have appeared to influence the work reported in this paper.

Acknowledgements

The authors would like to thank the European Union's Horizon 2020 research and innovation programme for funding this research under the GreenTRIBOS, Marie Skłodowska-Curie grant agreement No. 860246.

Appendix A. Supplementary data

Supplementary data to this article can be found online at https://doi.org/10.1016/j.compositesb.2025.112599.

Data availability

Data will be made available on request.

References

[1] Zanjanijam AR, Major I, Lyons JG, Lafont U, Devine DM. Fused filament fabrication of PEEK: a review of process-structure-property relationships. Polymers (Basel) 2020;12(8). https://doi.org/10.3390/polym12081665.
[2] Sikder P, Challa BT, Gummadi SK. A comprehensive analysis on the processing-structure-property relationships of FDM-based 3-D printed polyetheretherketone (PEEK) structures. Materialia 2022;22. https://doi.org/10.1016/j.mtla.2022.101427.
[3] Kurtz SM. PEEK biomaterials handbook. https://doi.org/10.1016/C2016-0-02479-8; 2019.
[4] Kurdi A, Chang L. Recent advances in high performance polymers—tribological aspects. Lubricants 2018;7(1). https://doi.org/10.3390/lubricants7010002.
[5] Rodzeń K, Harkin-Jones E, Wegrzyn M, Sharma PK, Zhigunov A. Improvement of the layer-layer adhesion in FFF 3D printed PEEK/carbon fibre composites. Compos Appl Sci Manuf 2021;149. https://doi.org/10.1016/j.compositesa.2021.106532.
[6] Li J, Fu Y, Pi W, Li Y, Fu S. Improving mechanical performances at room and elevated temperatures of 3D printed polyether-ether-ketone composites by combining optimal short carbon fiber content and annealing treatment. Compos. Part B: Eng 2023;267. https://doi.org/10.1016/j.compositesb.2023.111067.
[7] Lv X, Yang S, Pei X, Zhang Y, Wang Q, Wang T. Enhanced mechanical and tribological properties of 3D printed short carbon fiber reinforced polyether ether ketone composites. Polym Compos 2024;45(10):8840–60. https://doi.org/10.1002/pc.28380.
[8] Lv X, Yang S, Pei X, Zhang Y, Wang Q, Wang T. An investigation of the microstructure and tribological behavior of polyether ether ketone composites fabricated by extrusion-based additive manufacturing. Polym Int 2024;73(7):516–29. https://doi.org/10.1002/pi.6624.
[9] Dhakal N, Espejo C, Morina A, Emami N. Tribological performance of 3D printed neat and carbon fiber reinforced PEEK composites. Tribol Int 2024;193. https://doi.org/10.1016/j.triboint.2024.109356.
[10] Stepashkin AA, Chukov DI, Senatov FS, Salimon AI, Korsunsky AM, Kaloshkin SD. 3D-printed PEEK-carbon fiber (CF) composites: structure and thermal properties. Compos Sci Technol 2018;164:319–26. https://doi.org/10.1016/j.compscitech.2018.05.032.
[11] Matschinski A, Ziegler P, Abstreiter T, Wolf T, Drechsler K. Fiber Formation of printed carbon fiber/poly (ether ether ketone) with different nozzle shapes. Polym Int 2021;70(8):1109–17. https://doi.org/10.1002/pi.6196.
[12] Sommacal S, Matschinski A, Holmes J, Drechsler K, Compston P. Detailed void characterisation by X-ray computed tomography of material extrusion 3D printed carbon fibre/PEEK. Compos Struct 2023;308. 10.1016/10.1016/j.compstruct.2022.116635.
[13] Altıparmak SC, Yardley VA, Shi Z, Lin J. Extrusion-based additive manufacturing technologies: state of the art and future perspectives. J Manuf Process 2022;83:607–36. https://doi.org/10.1016/j.jmapro.2022.09.032.
[14] Pigliaru L, Rinaldi M, Ciccacci L, Norman A, Rohr T, Ghidini T, et al. 3D printing of high performance polymer-bonded PEEK-NdFeB magnetic composite materials. Funct. Compos. Mater. 2020;1(1). https://doi.org/10.1186/s42252-020-00006-w.
[15] Wang Y, Ulbricht A, Schmidt F, Muller BR, Kupsch A, Schwitalla AD. Micro-CT analysis and mechanical properties of low dimensional CFR-PEEK specimens additively manufactured by material extrusion. J Mech Behav Biomed Mater 2023;146:106085. 10.1016/10.1016/j.jmbbm.2023.106085.
[16] Rinaldi M, Ghidini T, Cecchini F, Brandao A, Nanni F. Additive layer manufacturing of poly (ether ether ketone) via FDM. Compos. Part B: Eng 2018;145:162–72. https://doi.org/10.1016/j.compositesb.2018.03.029.

[17] Berretta S, Davies R, Shyng YT, Wang Y, Ghita O. Fused Deposition Modelling of high temperature polymers: exploring CNT PEEK composites. Polym Test 2017;63:251–62. https://doi.org/10.1016/j.polymertesting.2017.08.024.
[18] Arif MF, Alhashmi H, Varadarajan KM, Koo JH, Hart AJ, Kumar S. Multifunctional performance of carbon nanotubes and graphene nanoplatelets reinforced PEEK composites enabled via FFF additive manufacturing. Compos. Part B: Eng 2020;184. https://doi.org/10.1016/j.compositesb.2019.107625.
[19] Yaragalla S, Zahid M, Panda JK, Tsagarakis N, Cingolani R, Athanassiou A. Comprehensive enhancement in thermomechanical performance of melt-extruded PEEK filaments by graphene incorporation. Polymers (Basel) 2021;13(9). https://doi.org/10.3390/polym13091425.
[20] Lv X, Pei X, Yang S, Zhang Y, Wang Q, Wang T. Tribological behavior of PEEK based composites with alternating layered structure fabricated via fused deposition modeling. Tribol Int 2024;199. 10.1016/10.1016/j.triboint.2024.109953.
[21] Díez-Pascual AM, Naffakh M, Marco C, Ellis G, Gómez-Fatou MA. High-performance nanocomposites based on polyetherketones. Prog Mater Sci 2012;57(7):1106–90. https://doi.org/10.1016/j.pmatsci.2012.03.003.
[22] Kuo MC, Tsai CM, Huang JC, Chen M. PEEK composites reinforced by nano-sized SiO2 and Al2O3 particulates. Mater Chem Phys 2005;90(1):185–95. https://doi.org/10.1016/j.matchemphys.2004.10.009.
[23] Zhang G, Schlarb AK, Tria S, Elkedim O. Tensile and tribological behaviors of PEEK/nano-SiO2 composites compounded using a ball milling technique. Compos Sci Technol 2008;68(15–16):3073–80. https://doi.org/10.1016/j.compscitech.2008.06.027.
[24] Guo L, Zhang G, Wang D, Zhao F, Wang T, Wang Q. Significance of combined functional nanoparticles for enhancing tribological performance of PEEK reinforced with carbon fibers. Compos Appl Sci Manuf 2017;102:400–13. https://doi.org/10.1016/j.compositesa.2017.09.002.
[25] Lin L, Schlarb AK. Development and optimization of high-performance PEEK/CF/Nanosilica hybrid composites. Polym Adv Technol 2021;32(8):3150–9. https://doi.org/10.1002/pat.5327.
[26] Lin L, Ecke N, Huang M, Pei X-Q, Schlarb AK. Impact of nanosilica on the friction and wear of a PEEK/CF composite coating manufactured by fused deposition modeling (FDM). Compos. Part B: Eng 2019;177. https://doi.org/10.1016/j.compositesb.2019.107428.
[27] ASTM. D792 - standard test methods for density and specific gravity (relative density) of plastics by displacement. https://doi.org/10.1520/D0792-20; 2020.
[28] ASTM. D2734 - standard test methods for void content of reinforced plastics. https://doi.org/10.1520/D2734-16; 2016.
[29] Blundell DJ, Osborn BN. The morphology of poly(aryl-ether-ether-ketone). Polymer 1983;24(8):953–8. https://doi.org/10.1016/0032-3861(83)90144-1.
[30] Dhakal N, Wang X, Espejo C, Morina A, Emami N. Impact of processing defects on microstructure, surface quality, and tribological performance in 3D printed polymers. J Mater Res Technol 2023;23:1252–72. https://doi.org/10.1016/j.jmrt.2023.01.086.
[31] Gao S-L, Kim J-K. Cooling rate influences in carbon fibre-PEEK composites. Part 1. Crystallinity and interface adhesion. Composites Part A 2000;31(6). https://doi.org/10.1016/S1359-835X(00)00009-9.
[32] Hay JN, Langford JI, Lloyd JR. Variation in unit cell parameters of aromatic polymers with crystallization temperature. Polymer 1989;30(3):489–93. https://doi.org/10.1016/0032-3861(89)90019-0.
[33] Langford JI, Wilson AJC. Scherrer after sixty years - a survey and some new results in the determination of crystallite size. J Appl Crystallogr 1978;11(2):102–13. https://doi.org/10.1107/S0021889878012844.
[34] Naganaboyina HPS, Nagaraju P, Sonaye SY, Bokam VK, Sikder P. In-house processing of carbon fiber-reinforced polyetheretherketone (CFR-PEEK) 3D printable filaments and fused filament fabrication-3D printing of CFR-PEEK parts. Int J Adv Des Manuf Technol 2023;128(11–12):5011–24. https://doi.org/10.1007/s00170-023-12203-5.
[35] Wang P, Zou B, Ding S, Huang C, Shi Z, Ma Y, et al. Preparation of short CF/GF reinforced PEEK composite filaments and their comprehensive properties evaluation for FDM-3D printing. Compos. Part B: Eng 2020;198. https://doi.org/10.1016/j.compositesb.2020.108175.
[36] Sosa-Rey F, Abderrafai Y, Diouf Lewis A, Therriault D, Piccirelli N, Lévesque M. OpenFiberSeg: Open-source segmentation of individual fibers and porosity in tomographic scans of additively manufactured short fiber reinforced composites. Compos Sci Technol 2022;226. https://doi.org/10.1016/j.compscitech.2022.109497.
[37] Hay JN, Kemmish DJ. Thermal decomposition of poly(aryl ether ketones). Polymer 1987;28(12):2047–51. https://doi.org/10.1016/0032-3861(87)90039-5.
[38] Lai YH, Kuo MC, Huang JC, Chen M. On the PEEK composites reinforced by surface-modified nano-silica. Mater Sci Eng, A 2007;458(1–2):158–69. https://doi.org/10.1016/j.msea.2007.01.085.
[39] Dawson PC, Blundell DJ. X-ray data for poly(aryl ether ketones).pdf>. Polymer 1980;21(5):577–8. https://doi.org/10.1016/0032-3861(80)90228-1.
[40] Rodzeń K, Sharma PK, McIlhagger A, Mokhtari M, Dave F, Tormey D, et al. The direct 3D printing of functional PEEK/hydroxyapatite composites via a fused filament fabrication approach. Polymers (Basel) 2021;13(4). https://doi.org/10.3390/polym13040545.
[41] Doumeng M, Berthet F, Delbé K, Marsan O, Denape J, Chabert F. Effect of size, concentration, and nature of fillers on crystallinity, thermal, and mechanical properties of polyetheretherketone composites. J Appl Polym Sci 2021;139(5). https://doi.org/10.1002/app.51574.
[42] Zhang G. Structure–tribological property relationship of nanoparticles and short carbon fibers reinforced PEEK hybrid composites. J Polym Sci B Polym Phys 2010;48(7):801–11. https://doi.org/10.1002/polb.21951.
[43] Menczel JD, Prime RB. Thermal analysis of polymers: fundamentals and applications. John Wiley & Sons, Inc.; 2009. https://doi.org/10.1002/9780470423837.
[44] Diez-Pascual AM, Xu C, Luque R. Development and characterization of novel poly(ether ether ketone)/ZnO bionanocomposites. J Mater Chem B 2014;2(20):3065–78. https://doi.org/10.1039/c3tb21800g.